Geoscientific
Model Development

Supplement of

Development of a sequential tool, LMDZ-NEMO-med-V1, to conduct global-to-regional past climate simulation for the Mediterranean basin: an Early Holocene case study

Tristan Vadsaria et al.

Correspondence to: Tristan Vadsaria (vadsaria@aori.u-tokyo.ac.jp, tristan.vadsaria@lsce.ipsl.fr)

The supplementary material includes:

- **Supplementary text**

Text S1: LMDZ-NEMO-med**,** user manual

Text S2: Bias correction

Text S2: Comparison of model simulation outputs with reconstructed data for the whole Mediterranean basin

- **Supplementary figures**

Fig. S1. Runoff of the Nile River

Fig. S2. Model/reconstruction data comparison for SST

Fig. S3. Model/reconstruction data comparison for SSS

Fig. S4. Time series of IS over the Mediterranean Sea in HIST

Fig. S5. Time series of maximum ZOF in the eastern Mediterranean Sea in HIST

Fig. S6. Time series of IS over the Mediterranean Sea in PICTRL and EHOL

Fig. S7. Time series of maximum ZOF in the eastern Mediterranean Sea in PICTRL and EHOL

Fig. S8. Time series of SSS for the Mediterranean Sea in PICTRL and EHOL

- **Supplementary tables**

Tab. S1. Model-data comparison for continental precipitation

Tab. S2. Forcings and parameters used in both AGCM and ARCM

Tab. S3. Forcings used in the ORCM

34   **Text S1: LMDZ-NEMO-med, user manual**

35

36   This section is intended as a user manual to explain how to compile and run LMDZ-NEMO-med on a
37   Linux system. It is not, however, a detailed description of the source code. Files relevant to the
38   running of the pre-industrial control simulation presented in the article have been archived and made
39   publicly available for downloading: https://zenodo.org/record/3258410 (Vadsaria et al., 2019).

40

41   1   Atmospheric global model

42   LMDz4, used here in both the global and regional versions, is version 4 of the LMDZ model. It has the
43   same major code structure and practical organization as what is consultable on the web page:
44   https://forge.ipsl.jussieu.fr/igcmg_doc/wiki/DocImodelBlmdz

45

46   1.1 Compiling the model

47   The compiling environment is MODIPSL, a convention for code compilation when the code is
48   distributed into different directories. The following directory should be consulted:

49   **"cd vadsaria_et_al_model/LMDZ_and_NEMOMED8_models/modipsl/util"**

50   Edit the "**AA_make.gdef**": the user should create a new entry to fit its computational architecture.
51   Compiler options have been set up in this file and will be propagated to "Makefile" at different places.

52

53   It is recommended that all previous configurations be cleared by typing "**./clr_make**". A new
54   configuration to match the right computer platform can then be created:

55   "**./ins_make -t NAME_OF_YOUR_ARCHITECTURE_SYSTEM**"

56   Before code compilation, the library netcdf and a Fortran compiler need to be installed. FCM (Flexible
57   Configuration Management: https://metomi.github.io/fcm/doc/), a tool developed by the UK Met
58   Office to manage the dependence among different subroutines of a complex code is also required.
59   Compiling options for FCM are stored under "machine/arch.path" and "machine/arch.fcm". They need
60   to be coherent with what stored under "**AA_make.gdef**" and "Makefile".

61   To compile the code, the following directory needs to be consulted:

62   **"cd vadsaria_et_al_model/LMDZ_and_NEMOMED8_models/modipsl/config/LMDZ"**

63   Then, with the help of "Makefile", the following can be compiled:

64   **"gmake lmdz96x71global"**

65   where "**lmdz96x71global**" is a keyword defined in the "**AA_make**" script allowing a configuration to
66   be chosen.

67   If the compilation is successful, then the executable codes "create_etat0_limit.e",
68   "make_relax_times.e" and "gcm.e" are stocked at the following directory:

69   **"cd vadsaria_et_al_model/LMDZ_and_NEMOMED8_models/modipsl/modipsl/bin"**

70

71   1.2 Running the model

72

73 The first step is the creation of boundary conditions for the global atmospheric model. The supporting
74 files needed for this step can be found in the following directory:

75 **"cd vadsaria_et_al_model/files_and_boundary_conditions_for_LMDZ_global/start_limit"**

76

77 A boundary condition file is already provided in this directory: "**limit_picontrol_debiais.nc**". It is
78 based on a bias-corrected file for SST and SIC data (following the procedure described in the main
79 article) derived from the IPSLCM5 model for the pre-industrial simulation. The procedure to generate
80 this boundary condition file is the following:

81   -   Prepare a netcdf file with SST and SIC bias-corrected data, interpolated on a 1°x1° grid: "**CM5-**
82   **piControl-pseudo_amip_1x1_tos_sic.3600-3699_climato.after_correction.nc**" (in the sub-
83   directory "/interpol", a code to generate a 1°x1° "AMIP" grid is provided :
84   "interpol_ipslcm5_amip_tos_sic.F90")

85   -   Create symbolic links:

86 **"ln –s CM5-piControl-pseudo_amip_1x1_tos_sic.3600-3699_climato.after_correction.nc**
87   **amipbc_sic_1x1.nc"**

88 **"ln –s CM5-piControl-pseudo_amip_1x1_tos_sic.3600-3699_climato.after_correction.nc**
89   **amipbc_sst_1x1.nc"**

90   -   Move the file obtained from the previous compilation of the model to the current directory and
91   execute:

92 **"./create_etat0_limit.e"**

93

94 This execution is based on a few ".nc" files containing information on topography, surface albedo, etc.
95 It also takes relevant information from definition files of the model (gcm.def, physic.def and
96 orchidee.def). It should create a "**limit.nc**" file.

97 After creating the initial states and boundary conditions, we are now ready to run the model with an
98 example from the following directory

99 **"cd vadsaria_et_al_model/files_and_boundary_conditions_for_LMDZ_global"**

100

101 The bash script "**launch_picontrol_run_global_type**" is an example of how to run the atmospheric
102 global model. The script firstly organizes files for boundary conditions and initial state (all presented
103 in the current directory), and then executes the model "**gcm.e**" to generate outputs. This script was
104 initially created for use in the supercomputing centre TGCC. It contains some TGCC-specific
105 instructions for the management of environmental variables, including the necessary pathways for the
106 model's preferences and allocation of computing resources. The script is executed with a time step of
107 one month.

108

109 To start the execution of the model:

110   ./**launch_picontrol_run_global_make 1**

111

112   "**1**" being the first month. It will create the **launch_picontrol_run_global_launcher** bash file. The
113   user should then execute this file according to the actual operating system. If the script works, it will
114   automatically generate the next iteration (the next month) until the maximum iteration is reached,
115   denoted as the "**stop**" variable in the "**launch_picontrol_run_global_type**" file, set here at 360
116   months (30 years).

117

118   2 Atmospheric regional model

119   2.1 Compiling the model

120   The code of this model is identical to that of the global version, but in "Makefile", the key word
121   should be changed from "lmdz96x71global" to "lmdz200120_oneway"

122   Go to the following directory:

123   "**cd vadsaria_et_al_model/LMDZ_and_NEMOMED8_models/modipsl/config/LMDZ**"

124   Then compile the code through Makefile:

125   **gmake lmdz200120_oneway**

126   where "**lmdz200120_oneway**" is a keyword defined in the "**AA_make**" script allowing a
127   configuration to be chosen.

128   If the compilation is successful, executable files are stored in the following directory:

129   "**cd vadsaria_et_al_model/LMDZ_and_NEMOMED8_models/modipsl/modipsl/bin**"

130

131   2.2 Running the model

132   The first step is to create the boundary conditions for the regional atmospheric model. A boundary
133   condition file, "**limit_picontrol_debiais.nc**", is already provided in the following directory:

134   "**/vadsaria_et_al_model/files_and_boundary_conditions_for_LMDZ_regional/start_limit**"

135   It is of course different from that of the global model, but it is also obtained from the same bias-
136   corrected SST and SIC data, derived from the IPSLCM5 global coupled model for the pre-industrial
137   simulation. The procedure to generate this boundary condition file is the same as described for the
138   global version.

139   To run the model, an example is given in the following directory

140   "**cd vadsaria_et_al_model/files_and_boundary_conditions_for_LMDZ_regional**"

141   The example bash script "**launch_picontrol_run_regional_type**" shows how to run the atmospheric
142   regional model. Unlike the global model, additional files are needed to nudge the regional model with
143   the global output. "**biline_poids_s.nc''**", "**biline_poids_u.nc**" and "**biline_poids_v.nc**" (presented in
144   the current directory) are interpolation files allowing efficient transformation of global variables for
145   the regional model grid. Nudged forcing, with a 2-hour time step, from the global model is stored in
146   "**sortie_histfrq.nc**.

147 Since the global and regional models share a common structure, their launch is also very similar,
148 although with different configuration files.

149

150 3 Mediterranean oceanic model

151 NEMOMED8 is the Mediterranean regional version of the NEMO ocean modelling platform.
152 Documentation of the model can be found at: http://forge.ipsl.jussieu.fr/nemo/wiki/Users

3.1 Compiling the model

154 The compilation of NEMOMED8 is managed entirely through MODIPSL, so the generation of
155 Makefile is the same as described earlier for LMDZ. The keyword to be used in the argument of
156 "gmake" is "nemomed8". The compilation procedure is simply the following:

157 **"cd vadsaria_et_al_model/LMDZ_and_NEMOMED8_models/modipsl/config/NEMOMED8"**

158 **"gmake nemomed8"**

159 **"cd vadsaria_et_al_model/LMDZ_and_NEMOMED8_models/modipsl/modipsl/bin"**

160 If the compilation is successful, then it creates the executable file, "**opa**". In our study, NEMOMED8
161 is compiled to run with 121 cores in parallel mode.

3.2 Running the model

163 Before running the model, the 3D boundary conditions for salinity and potential temperature over the
164 buffer zone in the Atlantic close to the Gibraltar need to be generated. This operation is conducted in
165 the following directory:

166 **"cd vadsaria_et_al_model/files_and_boundary_conditions_for_NEMOMED8"**

167 These boundary conditions are found in the files
168 "**data_1m_potential_temperature_nomask_picontrol_debiais_climato.nc**" and
169 "**data_1m_salinity_nomask_picontrol_debiais_climato.nc**", bias-corrected from the IPSLCM5 pre-
170 industrial simulation. The grid of the NEMOMED8 model ("**meshmask_med8.nc**") is provided
171 allowing the user to interpolate their own boundary conditions from this grid.

172 The second step is to generate the surface fluxes from the atmospheric regional model. For this
173 purpose, an interpolation is used to convert the LMDZ4 air-sea fluxes into the NEMOMED8 grid
174 (bilinear for wind stress and conservative remapping for other fluxes). For NEMOMED8, the water,
175 radiative, latent, sensible fluxes and wind stress are required. In the sub-directory "/lmdz_to_nemo", a
176 code is provided to generate the bilinear interpolation scheme:
177 "interpol_between_lmdz_et_nemo.F90". During the execution of the executable file, a weight file is
178 required ("opalmdmo", also provided in the sub-directory).

179 "**sst_picontrol_debiais.nc.000101**",

180 "**flx_picontrol_debiais.nc.000101**",

181 "**taux_picontrol_debiais.nc.000101**" and

182 "**tauy_picontrol_debiais.nc.000101**".

183 Finally, the bash script "**launch_picontrol_run_mediterranean_ocean_type**" is an example of the
184 instructions necessary to run the oceanic regional model. The procedure is similar to the global and
185 regional atmospheric model.

186

Text S2: Bias correction

The bias correction for our experiments driven by IPSL simulations is illustrated. IPSL-CM5A is a fully coupled climate system model. It operates autonomously for either present-day climate, future climate scenarios, or paleo climate reconstructions, depending on the external forcings or boundary conditions imposed on it. For its historical simulation of modern climate (from 1850 to 2005), we point out a few general biases that need to be corrected before running our regional system for paleo periods (Early Holocene). In the following, the bias-correction method for the oceanic 3-D structures, SST and SIC, as well as the freshwater discharges from rivers, is described.

SST and SIC global fields

The global fields of SST and SIC are the most important variables in our methodology since they contain the main climate change information to be transferred from global scale to regional scale. They are used to force both the AGCM and the ARCM. SST derived from IPSL-CM5A has a cold bias globally, which would exert strong impacts on the Mediterranean Sea and the nearby Atlantic region. To remove this bias, we simply applied an offset based on the difference between the IPSL-CM5A historical simulation and the ERA-Interim reanalysis (Dee et al., 2011) for the period 1970-1999.

IPSL-CM5A, on the other hand, tends to overestimate temperatures at the poles, which leads to an underestimation of the SIC. This bias affects the surface albedo and the global energy budget. It also affects the meridional temperature gradient and consequently the mid-latitude atmospheric eddies. The bias correction used for SIC is the analogue method presented in Beaumet et al. (2019). The basic idea is to adjust the total areas covered by sea ice for each hemisphere and for each month following the geographic and temporal biases. As with the previous corrections for SST, the hemispheric and monthly bias correction for SIC is based on the difference between IPSL simulations and observed SIC (Climatological monthly mean for 1970-1999 from ERA-Interim). Finally, the geographic distribution of SIC is determined by hemisphere and by month following an analogue relationship extracted to match observations from 1970 to 2012.

3D temperatures and salinities in the buffer-zone

The 3-D fields of oceanic temperature and salinity (over the whole water column) in the Atlantic buffer zone has been adjusted in the same way as for SST. We used the World Ocean Atlas (WOA) (Locarnini et al., 2013) as a reference to correct the outputs from the IPSL-CM5A historical simulation.

River runoff to the Mediterranean Sea

6

218   Freshwater discharge from rivers around the Mediterranean Sea is an important factor controlling the

219   overturning circulation of the Mediterranean. Due to the high sensitivity of oceanic circulation to this

220   variable, we decided to apply a bias-correction to calibrate the river discharges produced by LMDZ-

221   regional. Actually, the atmospheric model, coupled to the land surface model ORCHIDEE, tends to

222   overestimate the amount of freshwater runoffs compared to present-day observations (Figure S1). The

223   bias-corrected that we applied is based on the observed climatological runoff (Ludwig et al. 2009;

224   Vorosmarty et al., 1998) and the differences between the Early Holocene simulation and present-day

225   simulation. When the difference is relatively not significant, the corrected runoff is set to the

226   climatology, mainly to avoid negative values [1]. However, in order to stay consistent with the

227   methodology for SST and SIC bias correction, we chose the absolute difference correction method for

228   the river runoff.

229

230   Text S3: Comparison of model simulation outputs and reconstructed data for the Mediterranean
231   basin

232   *Continental precipitation*

233   The reconstructed data used for comparison with the EHOL simulation is taken from Dormoy et al.

234   (2009) for the Aegean Sea, from Peyron et al. (2011) for the Lake Accesa and Tenaghi Philippon, and

235   Magny et al. (2013) for Lake Pergusa. In these studies, continental precipitation is reconstructed based

236   on pollen sequences to emphasis the changes in precipitation seasonality. Several methods are used to

237   determine these changes. We chose to reconstruct these changes using the Modern Analogue Technique

238   (MAT, Guiot, 1990), because, in their study, Magny et al. (2013) compared their data to Peyron et al.

239   (2011). We extracted data values framing a few hundred years around 9.5 ka cal BP, consistent with

240   the orbital parameters of our atmospheric simulations (both global and regional). For the Northern

241   Sahara, data are based on $\delta^{18}O$ from Bar-Matthews et al.(2003).

242   Comparison between model outputs and reconstruction data in terms of annual and seasonality changes

243   can be conducted and anomalies against modern values can be shown. In winter, the model shows

244   positive precipitation anomalies for the four sites (Lake Accesa, model: 20-36 mm, data: 20-40mm,

245   Tenaghi Philippon, model: 30-45 mm, data: 10-35 mm, Aegean, model: 29-45 mm, data: 10-80mm,

246   Lake Pergusa, model: 7-26 mm, data: 35-60mm, Table S1). In summer, the model shows a more

247   contrasted response, with negative anomalies in summer temperatures (Table S1) due to the homogenous

248   drought (Fig 10d in the main article). However, this comparison cannot reflect the precipitation changes

249   for the entire continent. Indeed, in north of Lake Accesa we see positive summer anomalies (Fig 10d in

250   the main article).

---

[1] Namely, when the difference does not exceed 25%, of the annually average annual difference for the Nile river
runoff (due to the simulated amplitude, cf section 4.4) and 5% for the rest of the rivers.

251

Sea Surface Temperatures

253   We conducted a comparison of model output and data for SST as Adloff et al., (2011) did with the
254   reconstruction of Kucera et al., (2011) (unpublished work). This reconstruction is based on census
255   counts of foraminiferal species, and on the artificial neural network for the transfer function. The data
256   used span the Holocene Insolation maximum interval (8.5 - 9.5 ka BP). Winter SST values (January to
257   March, Figure S2, f) are a bit lower than the reconstruction especially for the Eastern basin (-1 to -2 °C).
258   The simulated summer SSTs (July to September, Figure S3, j) are higher between the Tyrrhenian Sea
259   and the Levantine Sea (+1 to +4 °C). This enhanced contrast between winter and summer values for
260   simulated SST produced an annual signal in good agreement with the reconstructed values (Figure S3,
261   c). Our results depict the same signal pattern as the simulations of Adloff et al. (2011) do, with some
262   differences in the enhanced seasonal contrast. In Figure S3 are also depicted the same climatology for
263   the bias Early Holocene SST and the bias corrected Early Holocene SST boundary conditions used in
264   the model architecture. This figure shows how the SST signal have been improved, from the bias
265   correction to the ORCM simulation, in order to range the reconstruction with the use of the regional
266   models.

267

Sea Surface Salinities

269   The comparison of SSS over the Mediterranean Sea provides an appropriate indicator of freshwater
270   perturbation induced by enhanced river fluxes. As a reference for comparison, we use a synthesis of SSS
271   sampled from the S1 deposition, and provided by Kallel et al. (1997). Our EHOL simulation takes the
272   Nile river enhancement into account, that is an annual river discharge of 13000 $m^3.s^{-1}$, against 2930 $m^3.s^{-1}$
273   for the pre-industrial value). The North-East rivers (Buyukmenderes, Vardar, Acheloos, Vjosa,
274   Semanit, Shkumbin, Durres, Mat and Drini) have their annual fresh water discharges increasing from
275   1082 $m^3.s^{-1}$ at pre-industrial level to 1622 $m^3.s^{-1}$. The fresh water discharge from February to May
276   increases even more, from 1619 $m^3.s^{-1}$ at pre-industrial level to 3228 $m^3.s^{-1}$ for EHOL. Our EHOL
277   simulation, even with a significant increase of freshwater inputs, still cannot reproduce a sufficient
278   decrease of SSS to match the reconstructed values, as shown in Figure S3. . Rohling (1999, 2000)
279   pointed out that this mismatch can be partly attributed to uncertainties in salinity reconstruction. It is not
280   always straightforward to interpret the isotopic composition of oxygen in terms of salinity. Finally, it is
281   likely that an additional non-negligible fresh water source is missing. To explain the substantial SSS
282   decrease, an additional source of freshwater associated with an amplification of the flux of the North
283   African rivers could potentially be superimposed on the Nile. Indeed, changes of this type in the
284   hydrology are clearly indicated by the data but are not reproduced in most of the Early and Mid-
285   Holocene simulations.
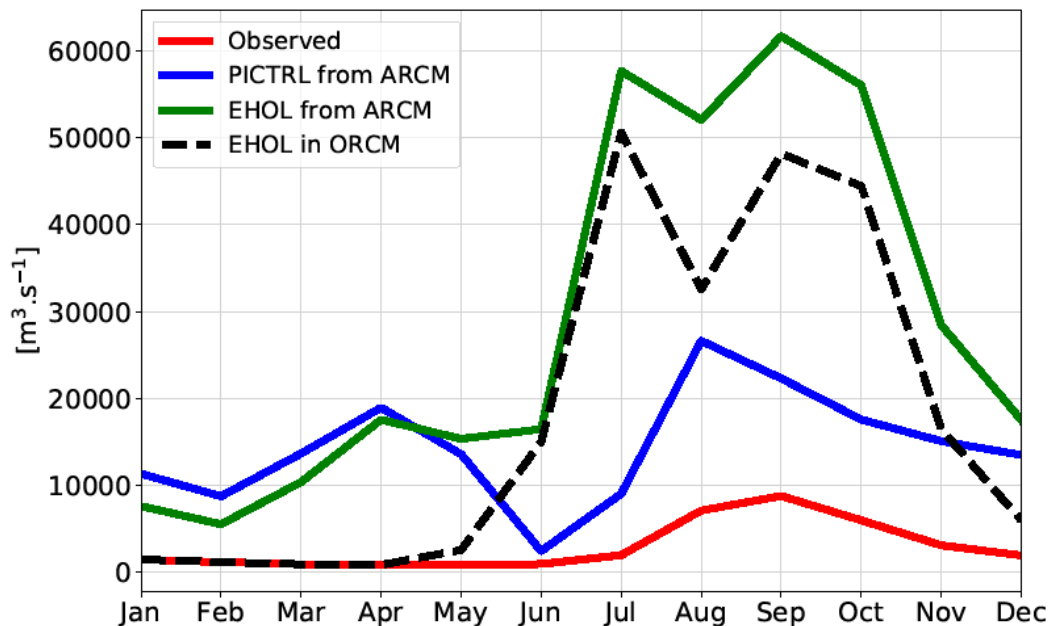
Figure S1: climatological runoff of the Nile River, observed pre-damming values (red), runoff as simulated by the ARCM, PICTRL (blue) and EHOL (green), and corrected runoff used in the ORCM.
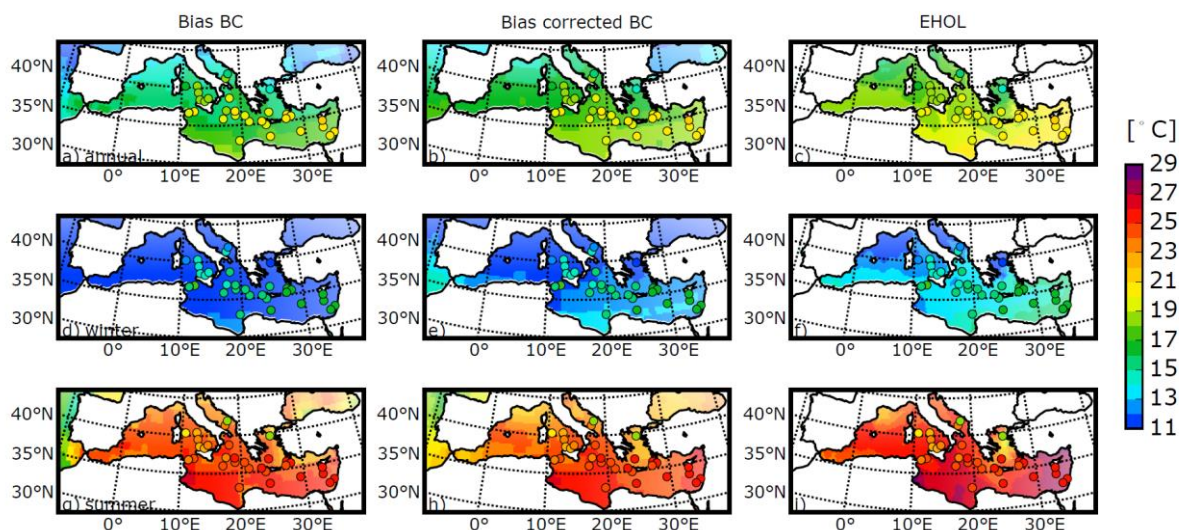

Figure S2: Model-data comparison for SST, adapted from Adloff (2011). Dots represent the unpublished synthesis of Kucera et al. (2011), published in Adloff (2011). The background colour represents, in the first column, the bias SST boundary conditions (BC) derived from the Early

298 **Holocene IPSL-CM5 simulation (AMIP resolution), in the second column, the bias corrected SST**

299 **BC as it has been used to drive the AGCM and the AGCM both (AMIP resolution), and, in the**

300 **third column, SST in the EHOL experiment realized with the ORCM (1/8°, averaged over the last**

301 **30 years of simulation).**

302
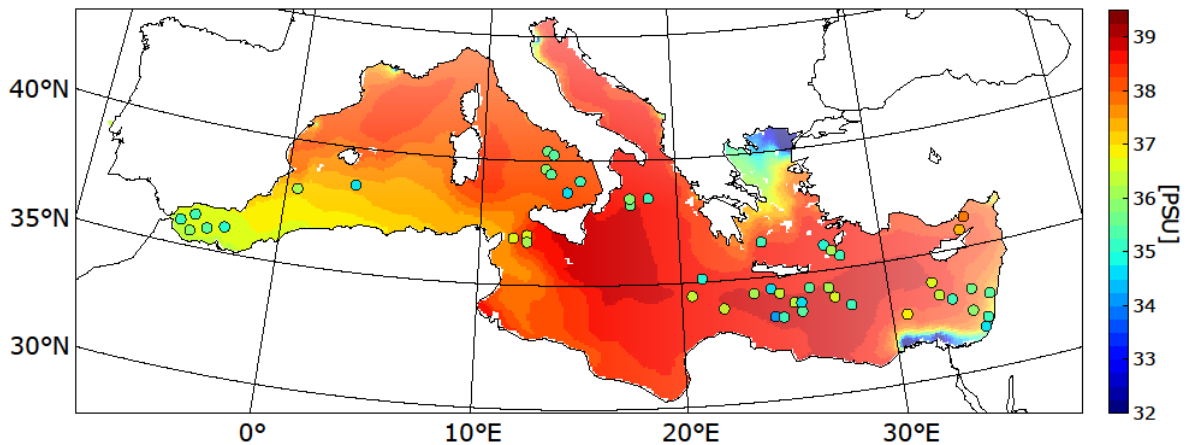
303

304 **Figure S3: Model-data comparison for SSS. Dots represent the synthesis of Kallel et al. (1997a).**

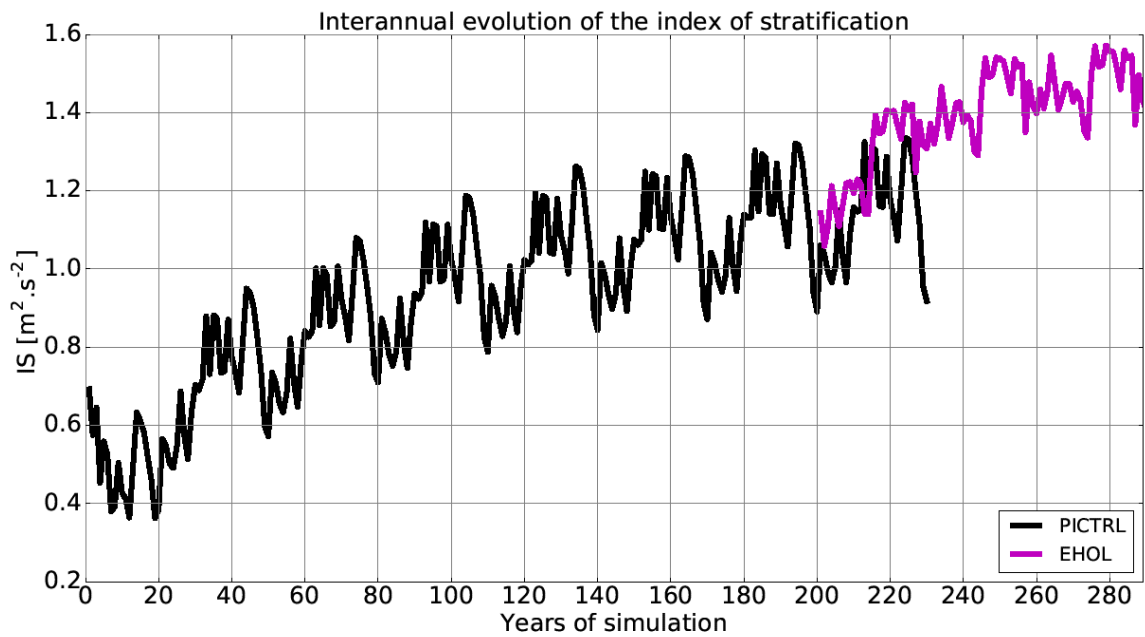305 **The background colour represents the EHOL simulation.**

306
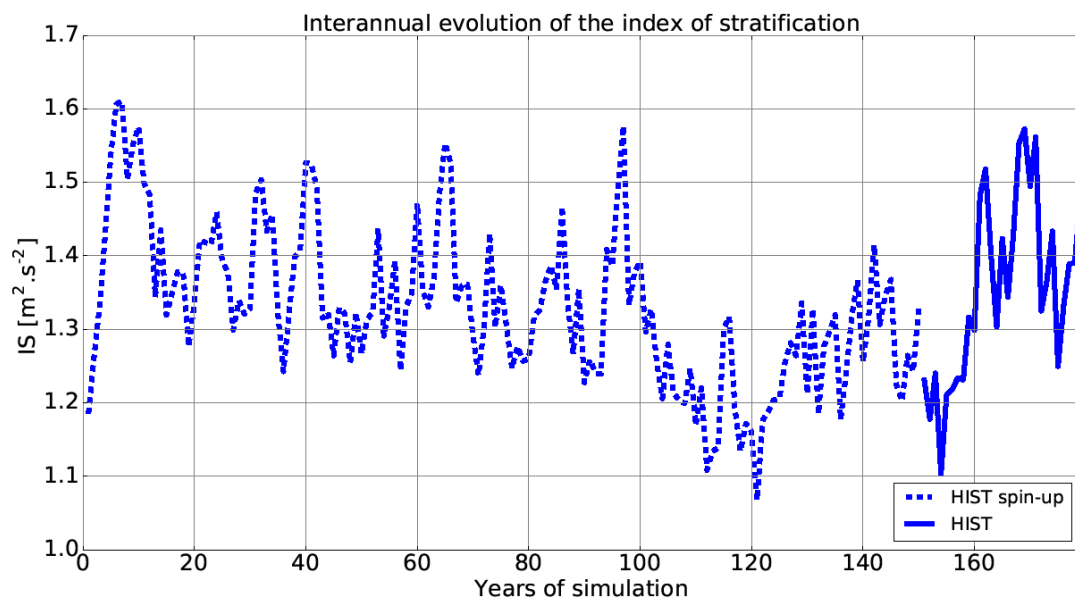
307

308 **Figure S4: Interannual evolution of the index of stratification (IS) for the Mediterranean Sea for**

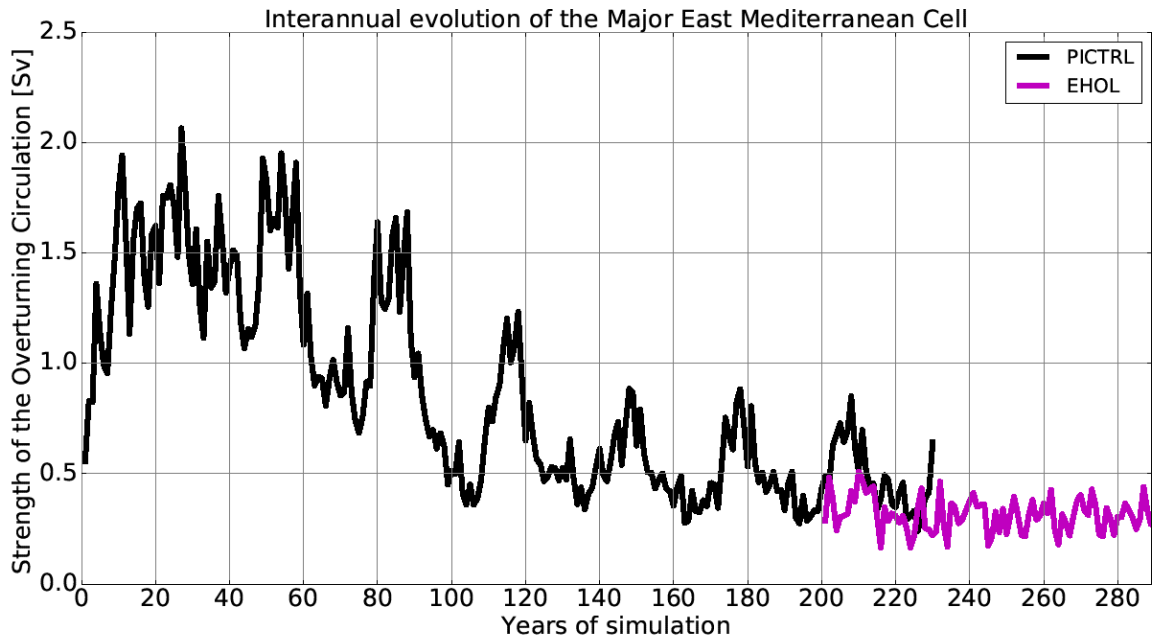309 **the HIST simulation (including the spin-up phase).**

310
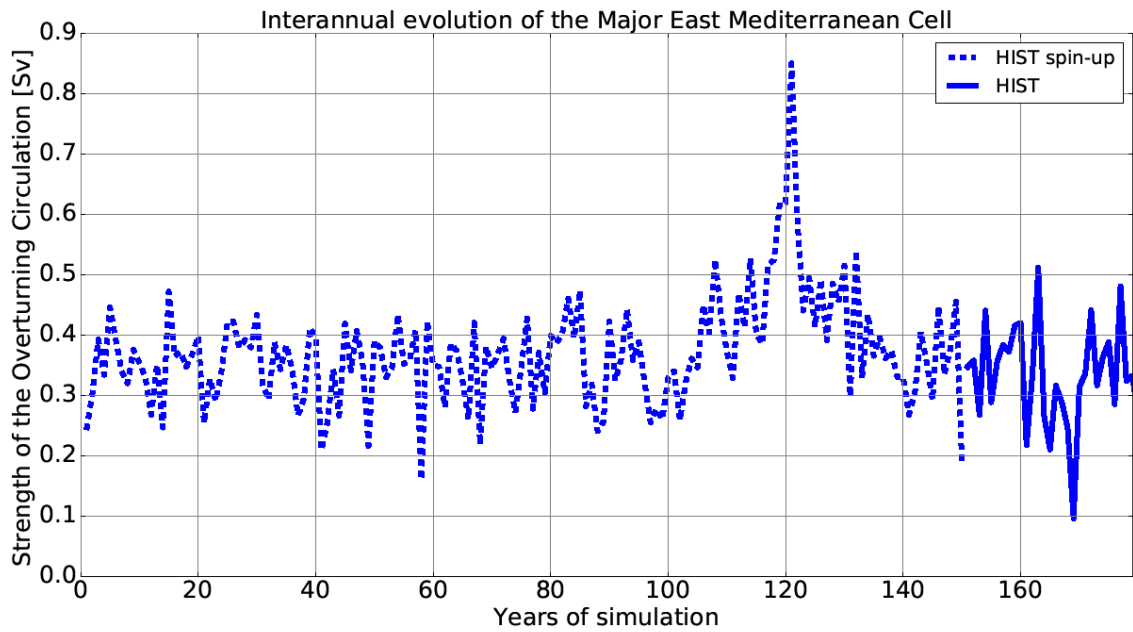
Figure S5: Interannual evolution of the Zonal overturning Stream Function (ZOF) in the eastern Mediterranean Sea for the HIST simulation (including the spin-up phase).
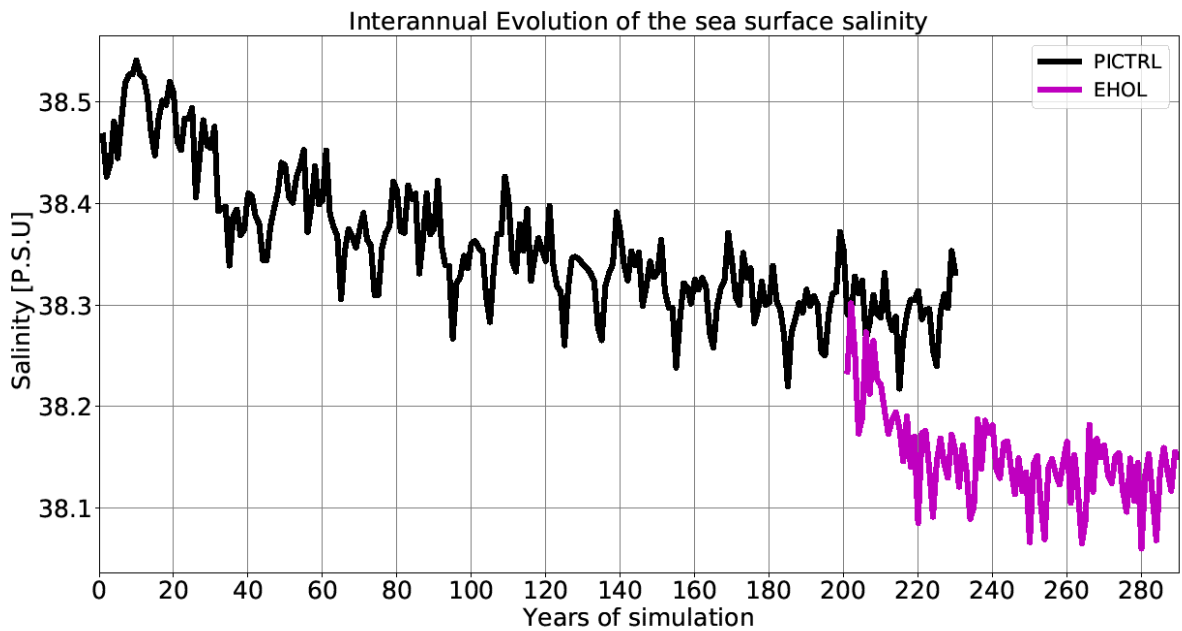

313

Figure S6: Interannual evolution of the index of stratification (IS) for the Mediterranean Sea for the PICTRL and EHOL simulations (including the PICTRL spin-up phase).

11

316

Figure S7: Interannual evolution of the Zonal overturning Stream Function (ZOF) in the eastern
Mediterranean Sea for the PICTRL and EHOL simulations (including the PICTRL spin-up
phase).

320

Figure S8: Interannual evolution of the sea surface salinity (SSS) for the Mediterranean Sea for
the PICTRL and EHOL simulations (including the PICTRL spin-up phase).

323

324

Precipitation (mm)	Winter			Summer			Annual		
	MODERN	ΔOBS	ΔEHOL	MODERN	ΔOBS	ΔEHOL	MODERN	ΔOBS	ΔEHOL
Lake Acessa	240	20-40	20-36	80	0-30	(-26)-(-8)	750	10-70	8-60
Tenaghi Philippon	225	10-35	30-45	80	20-50	(-13)-5	600	130-225	17-49
Lake Pergusa	225	35-60	7-26	80	30-50	(-17)-(-3)			
Aegean Sea	200	10-80	29-45	40	0-40	(-19)-0			
Northern Sahara							<200	700-800	(-20)-15

325

Table S1: Model-data comparison for continental. First row: Lake Accesa (Northern Italy) (Peyron et al., 2011), Second row: Tenaghi Philippon, (Greece) (Peyron et al., 2011), Third row: Lake Pergusa (Sicily), (Magny et al., 2013), Fourth row: Aegean Sea, (Dormoy et al., 2009), Fifth row: Northern Sahara (Bar-Matthews et al., 2003). "MODERN" refers to the present values of precipitation, "OBS" to the data (around 9.5 ka cal BP), and "EHOL" for the Early Holocene simulation described in the article.

	HIST	PICTRL	EHOL
Orbital parameters	e = 0.01672 ε = 23.44 ω -180 = 102.7	Same as in HIST	e = 0.01935 ε = 24.231 ω -180 = 303.3
Atmospheric CO_2	Annual observed global mean (1970-1999)	284 ppm	284 ppm
SST forcing	Era-Interim monthly forcing (1970-1999	IPSL-CM5A picontrol + SST correction	IPSL-CM5A early Holocene + SST correction
SIC forcing	Era-Interim monthly forcing (1970-1999	IPSL-CM5A picontrol + SIC correction	IPSL-CM5A Early Holocene + SIC correction

334

Table S2: Forcings and parameters used in both AGCM and ARCM. ε is the elliptic orbit obliquity, e, the eccentricity and ω, the longitude of the perihelion. The reader can notice that the

pCO$_2$ should be 260 ppm as suggested by the PMIP protocol for mid-Holocene. The goal in this paper was mainly to have a sensitivity to orbital parameters.

	HIST	PICTRL	EHOL
Buffer-zone T3D & S3D	WOA monthly forcing (1970-1999 mean)	IPSL-CM5A picontrol + T3D/S3D correction	IPSL-CM5A early Holocene + T3D/S3D correction
River runoff	Ludwig et al 2009, Rivdis database	Ludwig et al 2009, Rivdis database (But Pre-damming Nile)	Anomalies inferred from EHOL – PICTRL atmospheric simulations (NILE + East-North margin)

Table S3: Forcings used in the ORCM.

References

Adloff, F., Mikolajewicz, U., Kučera, M., Grimm, R., Maier-Reimer, E., Schmiedl, G. and Emeis, K. C.: Upper ocean climate of the Eastern Mediterranean Sea during the Holocene Insolation Maximum - A model study, Clim. Past, 7(4), 1103–1122, doi:10.5194/cp-7-1103-2011, 2011.

Bar-Matthews, M., Ayalon, A., Gilmour, M., Matthews, A. and Hawkesworth, C. J.: Sea - land oxygen isotopic relationships from planktonic foraminifera and speleothems in the Eastern Mediterranean region and their implication for paleorainfall during interglacial intervals, Geochim. Cosmochim. Acta, 67(17), 3181–3199, doi:10.1016/S0016-7037(02)01031-1, 2003.

Beaumet, J., Krinner, G., Déqué, M., Haarsma, R. and Li, L.: Assessing bias-corrections of oceanic surface conditions for atmospheric models, Geosci. Model Dev. Discuss., (December), 1–29, doi:10.5194/gmd-2017-247, 2017.

Dee, D. P., Uppala, S. M., Simmons, A. J., Berrisford, P., Poli, P., Kobayashi, S., Andrae, U., Balmaseda, M. A., Balsamo, G., Bauer, P., Bechtold, P., Beljaars, A. C. M., van de Berg, L., Bidlot, J., Bormann, N., Delsol, C., Dragani, R., Fuentes, M., Geer, A. J., Haimberger, L., Healy, S. B., Hersbach, H., Hólm, E. V., Isaksen, L., Kållberg, P., Köhler, M., Matricardi, M., Mcnally, A. P., Monge-Sanz, B.

359 M., Morcrette, J. J., Park, B. K., Peubey, C., de Rosnay, P., Tavolato, C., Thépaut, J. N. and Vitart, F.:
360 The ERA-Interim reanalysis: Configuration and performance of the data assimilation system, Q. J. R.
361 Meteorol. Soc., 137(656), 553–597, doi:10.1002/qj.828, 2011.

362 Dormoy, I., Peyron, O., Combourieu Nebout, N., Goring, S., Kotthoff, U., Magny, M. and Pross, J.:
363 Terrestrial climate variability and seasonality changes in the\rMediterranean region between 15 000 and
364 4000 years BP deduced\rfrom marine pollen records, Clim. Past, 5, 615–632, 2009.

365 Guiot, J.: Methodology of the last climatic cycle reconstruction in France from pollen data, Palaeogeogr.
366 Palaeoclimatol. Palaeoecol., 80(1), 49–69, doi:10.1016/0031-0182(90)90033-4, 1990.

367 Kallel, N., Paterne, M., Labeyrie, L., Duplessy, J. C. and Arnold, M.: Temperature and salinity records
368 of the Tyrrhenian Sea during the last 18,000 years, Palaeogeogr. Palaeoclimatol. Palaeoecol., 135(1–4),
369 97–108, doi:10.1016/S0031-0182(97)00021-7, 1997.

370 Kucera, M., Rohling, E. J., Hayes, A., Hopper, L. G. S., Kallel, N., Buongiorno Nardelli, B., Adloff, F.
371 and Mikolajewicz, U.: Sea surface temperature of the Mediterranean Sea during the early Holocene
372 insolation maximum, Clim. Past, 2011.

373 Locarnini, R. A., Mishonov, A. V., Antonov, J. I., Boyer, T. P., Garcia, H. E., Baranova, O. K., Zweng,
374 M. M., Paver, C. R., Reagan, J. R., Johnson, D. R., Hamilton, M. and Seidov, D.: World Ocean Atlas
375 2013, Volume 1: Temperature, NOAA Atlas., edited by S. Levitus and A. Mishonov., 2013.

376 Ludwig, W., Dumont, E., Meybeck, M. and Heussner, S.: River discharges of water and nutrients to the
377 Mediterranean and Black Sea: Major drivers for ecosystem changes during past and future decades?,
378 Prog. Oceanogr., 80(3–4), 199–217, doi:10.1016/j.pocean.2009.02.001, 2009.

379 Magny, M., Combourieu-Nebout, N., De Beaulieu, J. L., Bout-Roumazeilles, V., Colombaroli, D.,
380 Desprat, S., Francke, A., Joannin, S., Ortu, E., Peyron, O., Revel, M., Sadori, L., Siani, G., Sicre, M. A.,
381 Samartin, S., Simonneau, A., Tinner, W., Vannière, B., Wagner, B., Zanchetta, G., Anselmetti, F.,
382 Brugiapaglia, E., Chapron, E., Debret, M., Desmet, M., Didier, J., Essallami, L., Galop, D., Gilli, A.,
383 Haas, J. N., Kallel, N., Millet, L., Stock, A., Turon, J. L. and Wirth, S.: North-south palaeohydrological
384 contrasts in the central mediterranean during the holocene: Tentative synthesis and working hypotheses,
385 Clim. Past, 9(5), 2043–2071, doi:10.5194/cp-9-2043-2013, 2013.

386 Peyron, O., Goring, S., Dormoy, I., Kotthoff, U., Pross, J., de Beaulieu, J.-L., Drescher-Schneider, R.,
387 Vannière, B. and Magny, M.: Holocene seasonality changes in the central Mediterranean region
388 reconstructed from the pollen sequences of Lake Accesa (Italy) and Tenaghi Philippon (Greece), The
389 Holocene, 21(1), 131–146, doi:10.1177/0959683610384162, 2011.

390 Rohling, E. J.: Environmental control on Mediterranean salinity and δ 18 O, Paleoceanography, 14(6),
391 706–715, doi:10.1029/1999PA900042, 1999.

392   Rohling, E. J.: Paleosalinity: Confidence limits and future applications, Mar, Mar. Geol., 163, 1–11,

393   doi:10.1016/S0025-3227(99)00097-3, 2000.

394   Vadsaria, T., Li, L., Ramstein, G., & Dutay, J.-C.: Model and output for Vadsaria et al, "Development

395   of a sequential tool LMDZ-NEMO-med-V1 for global to regional past climate simulation over the

396   Mediterranean basin: an early Holocene case study", GMD publication. doi:10.5281/zenodo.3258409,

397   2019.

398   Vorosmarty, C. J., Feteke, B. M. and Tucker, B. A.: Global River Discharge, 1807-1991, V. 1.1

399   (RivDIS), 1998.

400